

Rice Husk Derived Activated Carbon/Polyaniline Composites As Active Materials For Supercapacitors

M.V. Lebedeva^{1,*}, A.B. Ayupov^{1,2}, P.M. Yeletsky¹, V.N. Parmon^{1,2}

¹ Boreskov Institute of Catalysis SB RAS, 630090 Novosibirsk, Lavrentieva Av., 5, Russia

² Novosibirsk State University, 630090 г. Novosibirsk, Pirogova str., 2, Russia

*E-mail: lebedeva@catalysis.ru

Received: 20 October 2017 / Accepted: 30 January 2018 / Published: 6 March 2018

Composite materials (CM) “carbon/polyaniline” were synthesized using porous activated carbon (AC) produced from carbonized rice husk, which has specific surface area $2265 \text{ m}^2\text{g}^{-1}$ measured by direct BET method. The series of the CM was synthesized by oxidative aniline polymerization method in the presence of the AC in acidic medium; polyaniline (PAni) content was varied from 18 to 60 wt. %. Electrochemical and properties of the CM were investigated by cyclic voltammetry, galvanostatic charge/discharge and stability tests. Results indicate that properties of the composites are governed by ratio of the components: a form of cyclic voltammogram curves and location of specific ox-red polyaniline peaks strongly depend on the PAni amount. Gravimetric capacitance grows with polymer content in the material and reaches maxima $465 \text{ F}\cdot\text{g}^{-1}$ in $1\text{M H}_2\text{SO}_4$ at discharge current density $0.2 \text{ A}\cdot\text{g}^{-1}$ for the sample with polyaniline content 60 wt. %. However, durability tests show that the most stable is the sample with the lowest (18 wt. %) polyaniline amount.

Keywords: Activated carbon, Composite materials, Polyaniline, Rice Husk, Synergetic effect.

1. INTRODUCTION

Among the various electrical energy storage devices, supercapacitors (SC) occupy an intermediate position between batteries and conventional capacitors. SCs exhibit unique energy characteristics, having a higher specific power than batteries, and at the same time, a higher specific energy compared to the conventional capacitors. Herewith, SCs have a long service life and low operating costs [1–3]. All these benefits attract great attention to the research and development of the new materials suitable for application in SCs.

Supercapacitors are usually classified according to a type of the energy storage: electric double layer capacitors and pseudocapacitors. In the first one, energy accumulation occurs on the electrode/electrolyte interface due to formation of the electric double layer (EDL). In pseudocapacitors,

energy is accumulated through the reversible ox-red reactions involving an used electrode material. In the both cases, structural and texture characteristics of the electrode material such as porosity, surface area, accessibility for electrolyte ions as well as surface chemistry are considered as determinant factors and influence on the final operating parameters.

The most used as electrode materials in SCs are carbon materials having a great variety of forms and modifications: porous carbons [4–7], [8,9], carbon nanotubes [10–13], graphene-based materials [14] etc. Energy accumulation in the carbon electrodes occurs predominantly via electric double layer charging that depends on surface area of the material used, which significantly restricts values of the specific capacitance. One of a promising way to increase amount of the energy stored is creation of composites based on materials, which accumulate energy through different mechanisms: EDL charge/discharge and pseudocapacitance. For instance, carbon material can be a stable conducting matrix and the second component can provide high values of specific capacitance. As such red/ox-active materials conducting polymers are being studied actively [15–19].

Polyaniline having high electronic conductivity in doped form and easily prepared by chemical and electrochemical methods is considered as promising material [20,21]. Specific capacitance of polyaniline electrodes can reach values more than one thousand Farads per gram depending on a method of preparation, doping level and experimental conditions. However, during the charge/discharge processes, the polyaniline structure undergoes cyclic swelling/contraction that leads to a gradual destruction of the polymer [22,23]. The use of carbon materials as the stable matrix allows stabilizing of the polymer on the carbon surface that can slow down its mechanical degradation significantly. Carbon/PAni composites prepared using various carbon materials such as carbon nanotubes [24,25], graphene [14,26–28], aerogels [21], activated carbons [29–31] have been studied comprehensive. Thus utilization of graphene allowed obtaining composites with superior gravimetric capacitance $1182 \text{ F}\cdot\text{g}^{-1}$ at $1 \text{ A}\cdot\text{g}^{-1}$ [27] and a high electrochemical stability without any capacitance loss. However graphene synthesis is complicated and required high qualification [32]. Furthermore, graphene expensiveness hinders its commercial application that requires a large-scale production.

The use of biomass-derived ACs, due to simplicity of their production and low cost is much more attractive. High-ash biomass, such as rice husk (RH) that contains 13 – 29 wt. % of silica can be considered as a natural template-containing precursor [33]. Previously, we reported on characterization of ACs synthesized from RH carbonized in fluidized catalyst bed reactor followed by KOH activation [34,35]. These carbons are characterized by unique porous structure with small micropore fraction (< 40 %) and expanded surface up to $2500 \text{ m}^2\cdot\text{g}^{-1}$. Studies of capacitive properties of the ACs showed that their formed porous structure provides a good diffusion of electrolyte ions and values of specific capacitance are retained up to high charge/discharge rate (at current density changing from 0.1 to $2 \text{ A}\cdot\text{g}^{-1}$, 15 % of capacitance loss was observed [36]). Thus, AC with A_{BET} surface area $2265 \text{ m}^2\cdot\text{g}^{-1}$ and high gravimetric capacitance $230 \text{ F}\cdot\text{g}^{-1}$ has been chosen as a porous matrix for the polyaniline deposition. A series of the “activated carbon/conducting polymer” composite materials with various ratios of the components has been prepared. The composites were prepared by oxidative polymerization and studied by a set of physic-chemical methods.

2. EXPERIMENTAL

2.1. Synthesis of the activated carbon

The activated carbon sample was prepared from RH carbonized in fluidized catalyst bed reactor by alkali activation, accordingly to [34,35]. In brief, RH (ash content 19.5 wt %) grounded to particles of size < 1 mm was carbonized in the reactor with fluidized bed of deep oxidation catalyst (IK-12-73, SKTB Katalizator Ltd.) at 465 °C and estimated contact time 0.3-0.4 s. As a result, porous carbon-silica composite ($A_{\text{BET}} = 180 \text{ m}^2 \cdot \text{g}^{-1}$ and ash content 59.6 wt. %) was produced. This composite was further mixed with KOH flakes (high purity grade, GOST 24363-80) in mass ratio 4 (KOH) to 1 (carbonized RH). The thermal treatment of the mixture was performed in a static stainless steel reactor with heating rate $5 \text{ }^\circ\text{C min}^{-1}$ up to 890 °C. When achieving the temperature, the reactor heater was switched off with its following gradual cooling down. After the activation, the obtained mixture of the synthesized AC and formed alkali impurities (potassium silicates, carbonate, admixtures from reactor material etc.) was dissolved in an excess of deionized water, the produced AC material was further thoroughly washed till neutral pH. Then the AC sample was dried in an oven at 120 °C overnight to constant weight.

2.2. Synthesis of carbon/polyaniline composite material

The composite materials were synthesized through the oxidative aniline polymerization method in the presence of the AC in acid media. Aniline and the RH-derived were premixed in 0.1 M hydrochloric acid for half an hour, then the mixture was cooled down to 5 °C in an ice bath followed by a dropwise addition of ammonium persulphate $(\text{NH}_4)_2\text{S}_2\text{O}_8$ aqueous solution under vigorous stirring. The resulting material was washed out several times with of 0.1 M solution of hydrochloric acid to remove unreacted components. The sample was then dried in the oven at 80 °C for 6 h. Pure polyaniline was synthesized by the same procedure as well.

2.3. Characterization methods

Porous structure of the polyaniline, the AC and their composite were characterized with nitrogen adsorption at 77K. Isotherms of the nitrogen adsorption were measured by means of a Quadrasorb EVO (Quantachrome Instruments) analyzer of surface area and pore size. Prior to measurements, all samples were degassed under vacuum to remove moisture and other adsorbed contaminates. To avoid melting of the polymer and with their subsequent re-distribution in pores of the support, samples of polymers and composites were outgassed at 70 °C for 10 h. Samples of the AC were pretreated at 300°C for 10 h. The surface area was calculated by standard BET method according to IUPAC recommendations [37] and by direct BET calculation method to avoid errors due to capillary condensation in narrow mesopores as large as 3 nm in diameter [38]. The pore size distribution was computed by means of QSDFT equilibrium model for the nitrogen adsorption in slit-like pores at 77K using the software supplied with the instrument.

The CHNS elemental composition of the composite materials was determined using a VARIO EL CUBE CHNS-O analyzer (Elementar Analysensysteme, Germany). Each of the samples was analyzed at least three times with subsequent averaging of the results.

HRTEM study was performed by means of electronic microscope JEM-2010 (JEOL, Japan). Particles of studied samples were deposited by an ultrasound disperser on the copper perforated substrate.

2.4. Electrode preparation and electrochemical measurements

To prepare the working electrode, a mixture of the sample, carbon black and polytetrafluoroethylene (PTFE) in a ratio 8.5:1:0.5 in water with a few drops of isopropanol was treated in an ultrasonic bath for 10 min. The PTFE was used as binder and carbon black as conductive additive. Then, the obtained mixture was dried in the oven at 80 °C for 5 h. Working electrodes in the form of 1 cm diameter pellets (*ca.* 6-7 mg) were obtained by pressing the mixture. The experiments were performed in a three-electrode cell in 1 M H₂SO₄ as an electrolyte. As a counter electrode, the high-surface tableted AC was used; Hg/HgSO₄ electrode was used as reference electrode. All values of potential in this article are reported versus reversible hydrogen electrode (RHE). Electrochemical measurements were performed using a potentiostat/galvanostat Autolab PGSTAT 30. Electrochemical characteristics of electrodes were examined by cyclic voltammetry at 1 mV·s⁻¹ scan rate and chronopotentiometry at current densities from 0.2 to 5.0 A·g⁻¹. Investigation of the stability of electrodes was carried out by chronopotentiometry methods at current density 3 A·g⁻¹ for 1000 cycles.

3. RESULTS AND DISCUSSION

3.1. HCNS-analysis data

The use of rice husk having the high content of the silica (19.5 wt. %) that plays a role of a natural mineral template allows synthesis of AC with a small fraction of micropores and high BET specific surface area (Table 2, Figure 3). Thus, a considerable amount of the polymer can be supported onto the AC selected. The data of HCNS elemental analysis of the composite materials are presented in Table 1. Samples are designated according to the aniline amount calculated for the synthesis.

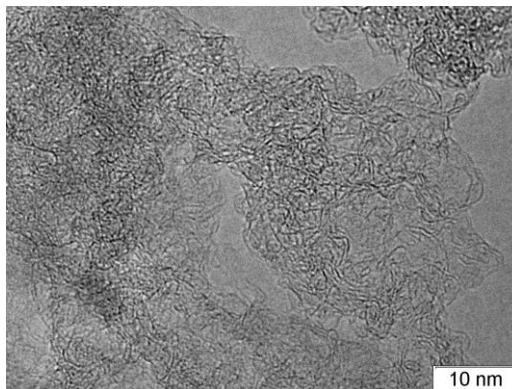
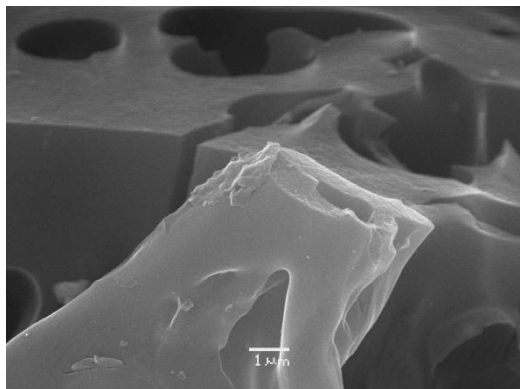
Table 1. Polyaniline content in the composite materials

CM sample	Calculated for synthesis quantity of PAni, %	Real quantity of PAni in the sample*, %
CPAn-20	20	18.4
CPAn-45	45	37.3
CPAn-60	60	47.8
CPAn-80	80	60.7

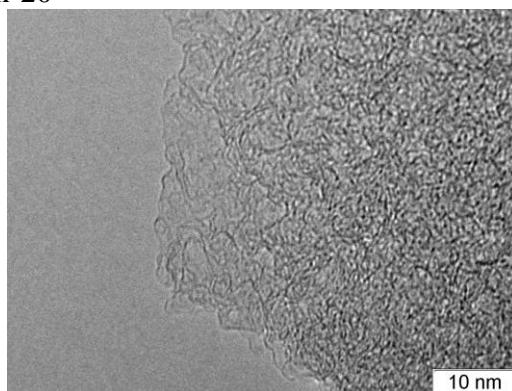
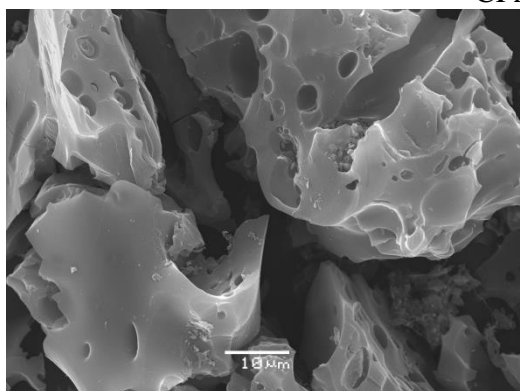
* - calculated from the HCNS-analysis data

For all synthesized samples, there is a trend of the polymer content decreasing in the final product as compared to the aniline quantity calculated for the synthesis. As polyaniline content in CMs increases, the difference between initial and obtained carbon/polymer ratio increases as well. This may be connected with the fact that when higher quantities of the supported polymer are used, the surface available for the monomer sorption is reduced, and significant amount of the polymer is become to be not bound with the AC surface and thus washed out during the washing process.

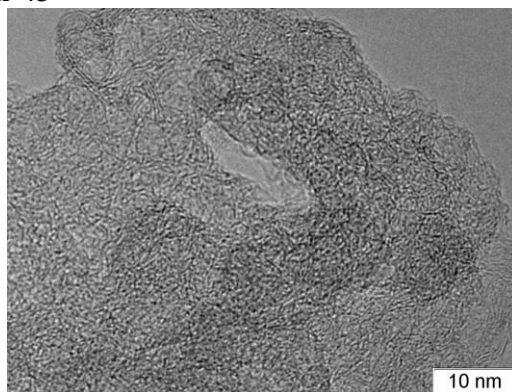
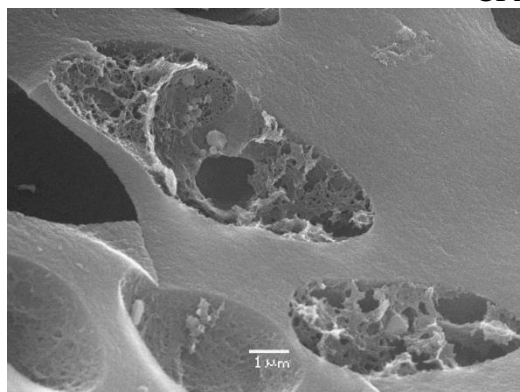
Carbon



CPAn-20



CPAn-45



CPAn-60

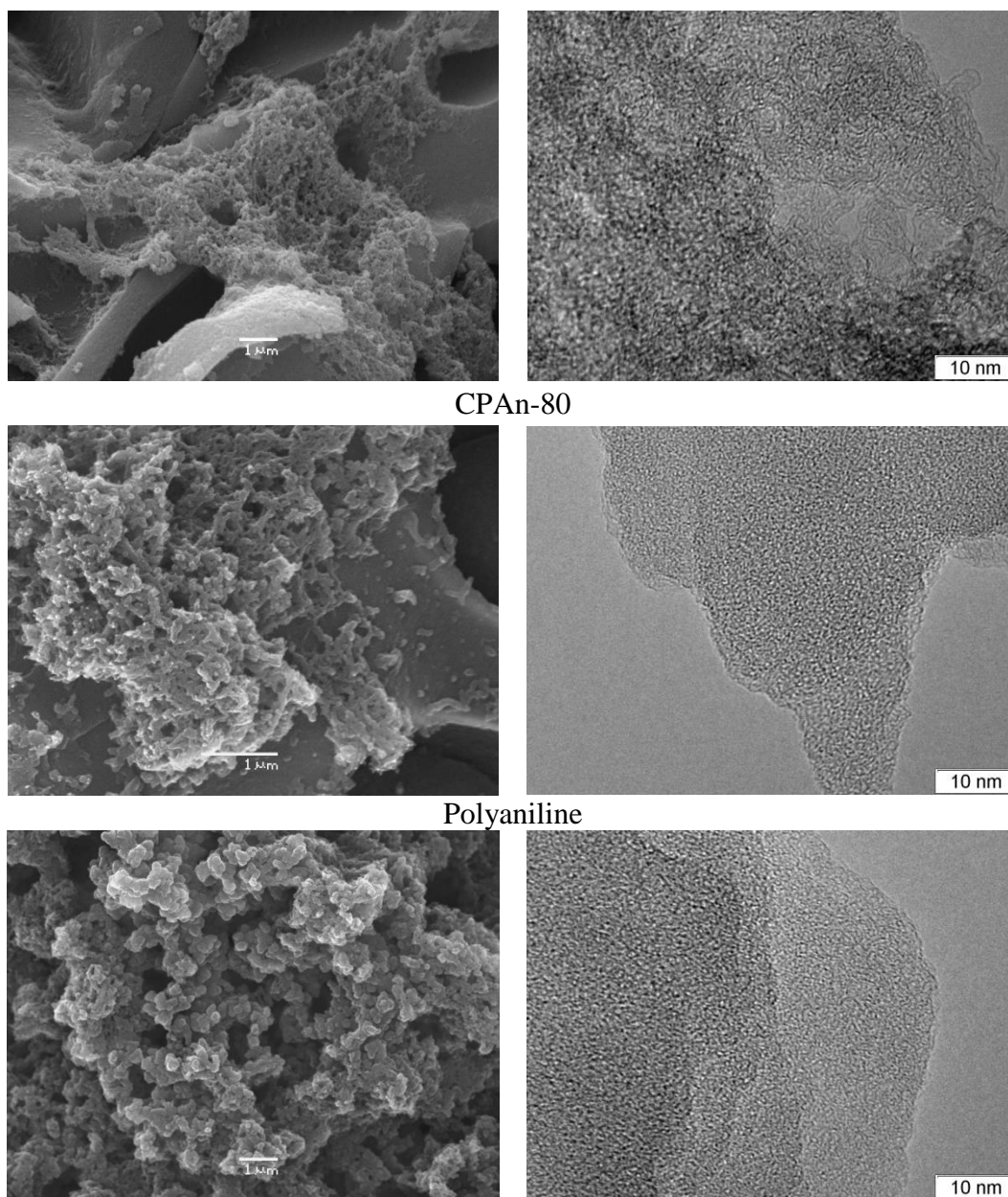


Figure 1. Typical TEM and SEM images of the RH-derived AC, polyaniline and /PANi/AC composites

Morphologies of the AC, polyaniline and CMs were investigated by scanning and transmission electron microscopies. The results are presented in the Figure 1.

Based on the TEM-study, the surface of the CPAn-20 sample is similar to that of AC. Changes caused by polyaniline presence are hardly differentiated. The presence of darkened areas on the surface is not directly correlated with the polymer coating. However based on elemental analysis the sample contains 18% of the PANi and its presence is confirmed by the electrochemical data as well. On TEM images of the CPAn-45 containing two times more polyaniline than CPAn-20, the carbon and polyaniline areas are clearly distinguished. Further increasing of the polyaniline content leads to reduction of the uncovered carbon surface and in the CPAn-80 sample with the highest polyaniline loading the surface is sample completely covered by the polymer.

Deposition of polyaniline on the carbon surface changed the polymer morphology, as seen from the SEM study. Pure polyaniline represents a globular structure with 200-300 nm globule size linked together to form a net with pores of diameter about 1 μm . Structure of the polymer on the carbon surface is changed with the polymer quantity.

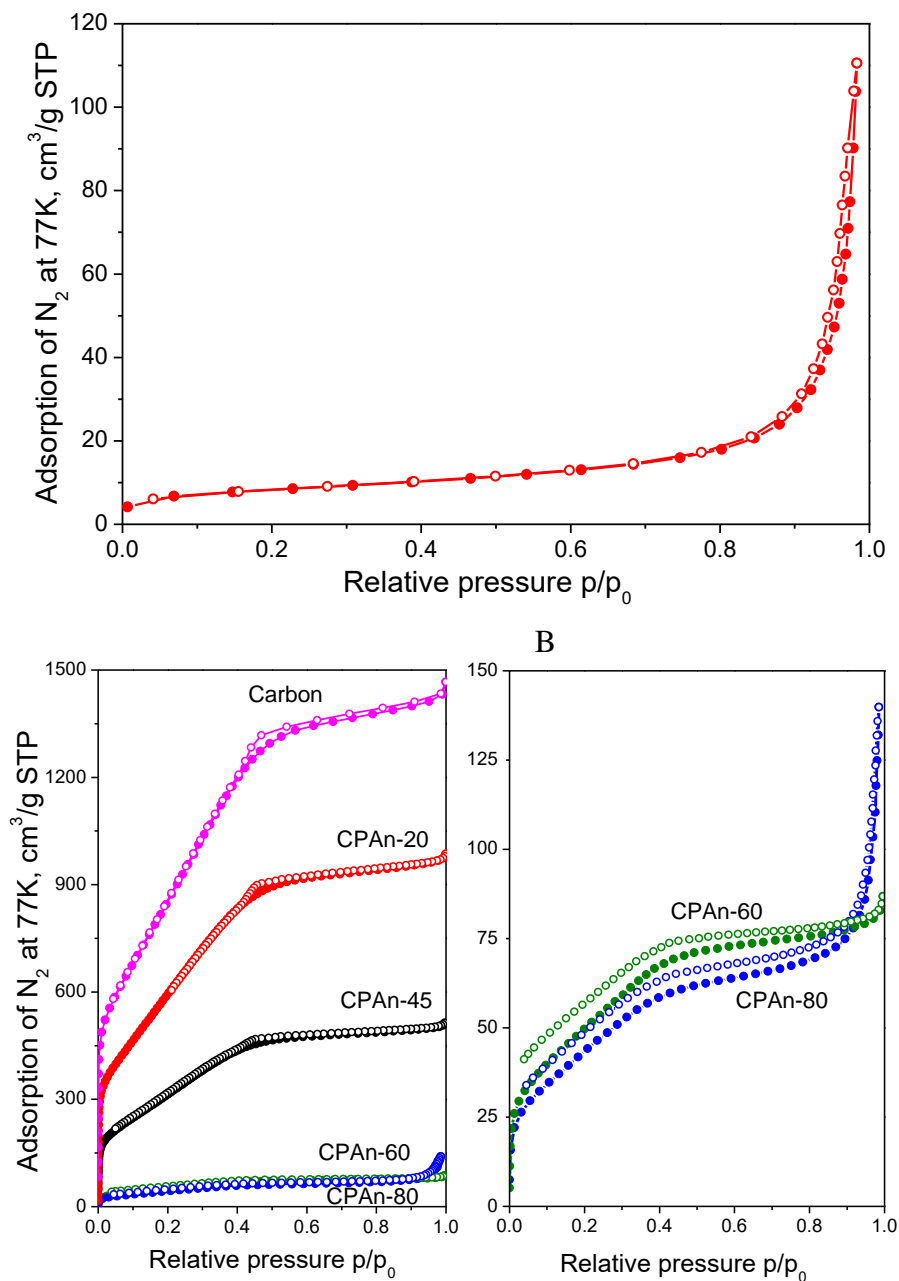


Figure 2. A - Isotherm of nitrogen adsorption on polyaniline; B - Isotherms of nitrogen adsorption on polyaniline/carbon composites and AC. The adsorption is given by closed symbols, desorption - by opened symbols

As in the case of TEM images, SEM images of CPAn-20 do not reflect any difference between carbon and polymer. On the surface of CPAn-45 containing 37% wt. % of PANi, the polymer forms net-like structure in the cavities of the carbon. On the CPAn-60 surface, the polymer is located not only in the cavities but through surface on the carbon: there are polymer islands and rods connected

together having diameter *ca.* 100nm. In the case of CPAn-80 containing about 60 wt. % of polyaniline, it forms 3D structure similar to pure polyaniline but with less geometrical dimensions.

Nitrogen adsorption isotherms on the ACCMs and polyaniline are presented in Fig. 2. The nitrogen adsorption isotherm corresponding to polyaniline is close to typical isotherms of Type II according to IUPAC classification [37], which is characteristic for non-porous samples or the ones with very wide pores.

It can be seen that the isotherms of the composite samples as well as of the carbon material are of Type IV(b) [37], which is characteristic for mesoporous materials with pore diameter or width less than 4-5 nm. It was found that CPAn-60 and CPAn-80 samples show some specific features. Adsorption and desorption branches of their isotherms are not following each other even at low pressure. Such a feature is sometimes observed in nitrogen adsorption on compliant materials such as flexible or microporous polymers, carbon or silica aerogels and could be explained by swelling of such materials [39] and trapping of nitrogen due to restricted pore access during the desorption [40]. At higher relative pressures, the isotherms show the increase in adsorption that can be attributed to higher content of polyaniline in these samples.

Pore size distributions (PSD) given in Fig.3 show that all the samples, except the polyaniline, are micro-mesoporous - the size of the most of pores in these samples are less than 5 nm.

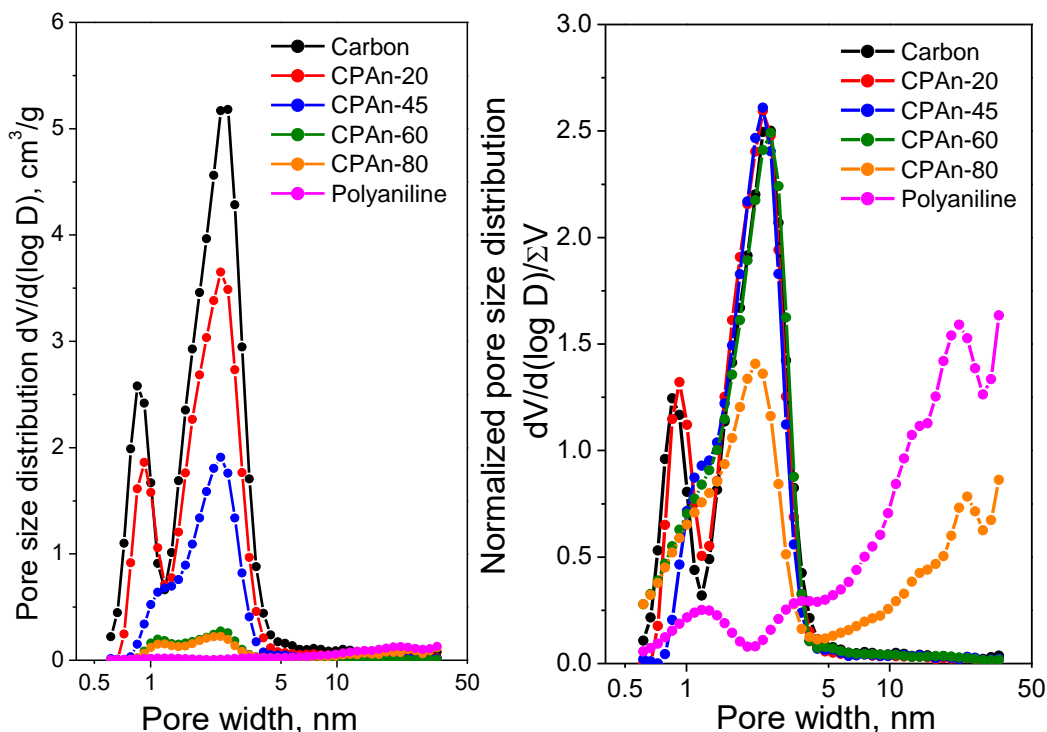


Figure 3. Pore size distributions $dV/d(\log D)$ in samples of polyaniline, polyaniline/carbon composites and highly porous carbon support. Left: PSD “as is”, right: the normalized to the total pore volume ($D < 35$ nm)

Characteristics of porous structure of the samples are summarized in Table 2.

Table 2. Characteristics of porous structure of AC, polyaniline and CMs.

Sample	Specific surface area by BET (IUPAC), $\text{m}^2 \cdot \text{g}^{-1}$	Specific surface area by direct method BET, $\text{m}^2 \cdot \text{g}^{-1}$	Specific surface area by QSDFT, $\text{m}^2 \cdot \text{g}^{-1}$	Micropore volume (QSDFT), $D < 2\text{nm}$, $\text{cm}^3 \cdot \text{g}^{-1}$	Total pore volume (QSDFT), $D < 35\text{nm}$, $\text{cm}^3 \cdot \text{g}^{-1}$
AC	3429	2265	2392	0.95	2.08
CPAn-20	2408	1608	1571	0.67	1.41
CPAn-45	1265	847	945	0.36	0.73
CPAn-60	192	152	124	0.073	0.12
CPAn-80	172	142	109	0.059	0.14
Polyaniline	30.1	30.8	25.3	0.0071	0.080

Increasing the polyaniline content yields a decrease in specific surface area (SSA) and total pore volume (TPV) of the composites. AC and CPAn-20 have little differences in PSD although SSA and TPV in CPAn-20 sample are lower than those of carbon. These two samples have a bimodal pore size distribution $dV/d(\log D)$ with modes at 0.9 and 2.6 nm. Samples CPAn-45, CPAn-60 and CPAn-80 show a different PSD: in their pore size distribution $dV/d(\log D)$ the mode at 0.9 nm disappears thus transforming to a peak shoulder with an inflection point at 1.3 nm. This indicates that polyaniline completely covers pores less than 1 nm. Peak shoulder at 1.3 nm can be connected with polyaniline porous structure since it has pronounced mode at this value and the samples contains significant amount of the polymer. CPAn-80 demonstrates an increase in the share of the pores wider than 5 nm, which is connected with large amount of the PANi forming 3D porous polymer structure.

3.2. Electrochemical properties of activated carbon and polyaniline

Cyclic voltammetry curves (CVA-curves) of the activated carbon and polyaniline are shown in Figure 4.

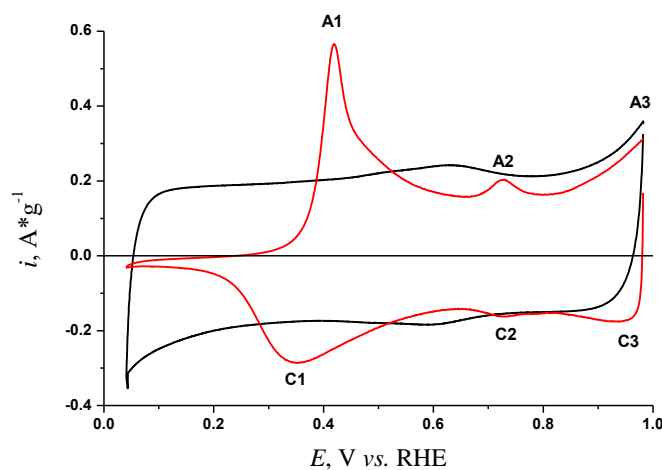


Figure 4. Cyclic voltammetric curves of the AC (black line) and polyaniline (red line). The scan rate is $1 \text{ mV} \cdot \text{s}^{-1}$, electrolyte is $1 \text{ M H}_2\text{SO}_4$

CVA-curve of the carbon has symmetric near rectangular shape, characteristic for this type of the materials. Pair of the weak reversible peak (about 0.6 V) on the CV curve is associated with quinone/hydroquinone couples on the carbon surface [41]. The intensity of the currents caused by the occurrence of ox-red reactions involving these groups is small compared to EDL-connecting currents. This behavior indicates that the energy accumulation in AC is mainly due to the charging/discharging of the electric double layer.

Shape of the polyaniline CVA-curve is characteristic to this polymer in acidic medium [20,42–44]. On the curve, two regions are clearly distinguished differentiated by the detected current intensity. In the potential region up to ~ 0.3 V, the current intensity is insignificant; the sharp increase begins after 0.4 V. A pair of peaks at 0.42/0.35 V (A1/C1) corresponds to the red-ox transition between different forms of the polyaniline: leucoemeraldine (semiconducting form of the polymer) and emeraldine (conductive one). This is reflected in the sharp growth of detected current during formation of the conducting form [20,45–47]. Peak A3/C3 formed when oncoming to 1 V is associated with formation (anodic branch) and reduction (cathodic branch) of the most oxidized polyaniline form – pernigraniline. The pair of peaks A2/C2 at 0.72/0.73 V appeared on the second scan (shown in Fig. 4) referred to the oxidation/reduction of *p*-benzoquinone/hydroquinone pair - soluble products of pernigraniline electrochemical degradation via hydrolysis [22,23,45,48]. It is accompanied by shortening of the polymer chains and by increasing of the resistance [49]. At the prolonged cycling above 0.8 V potential, quality of the polymer deteriorates with its gradual destruction. For the further investigations, the upper potential limit 0.8 V was chosen to slow down the polyaniline degradation.

Thus, the lower threshold of ~ 0.4 V and the upper one ~ 0.8 V limit the working potential window where polyaniline acts as an effective and stable energy accumulating material.

3.3. Electrochemical properties of the composite materials

To study the electrochemical properties of synthesized composite materials, the CVA-curves in 1 M sulfuric acid were recorded. The obtained data are presented in Figure 5.

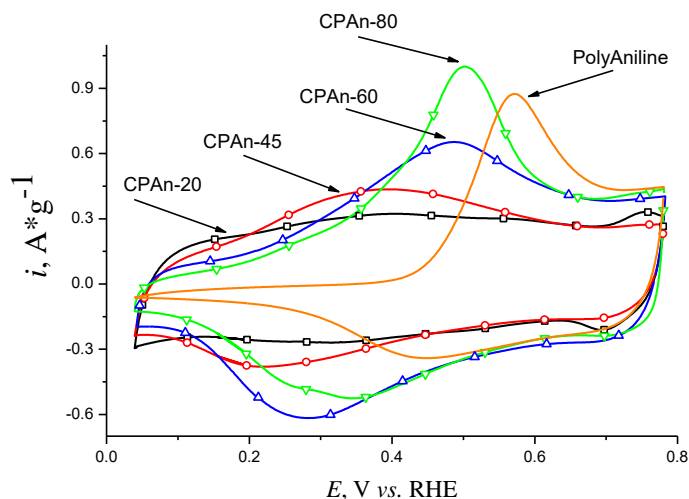


Figure 5. Cyclic voltammogram of the carbon/polyaniline composite materials with different ratios of the components. The scan rate is $1 \text{ mV} \cdot \text{s}^{-1}$, electrolyte – $1 \text{ M H}_2\text{SO}_4$

The polymer inclusion into CMs results in a gradual change of the CVA-curve shape. On the CVA-curves of the composites in potential range up to ~ 0.2 V, current intensity decreases with increasing in the polymer content. Since in this potential interval an electrochemical response is determined mainly by the carbon material itself, the decrease in the current intensity indicates that polyaniline partially blocks carbon surface, which is confirmed by TEM, SEM and N_2 adsorption data as well (Fig. 1, 3).

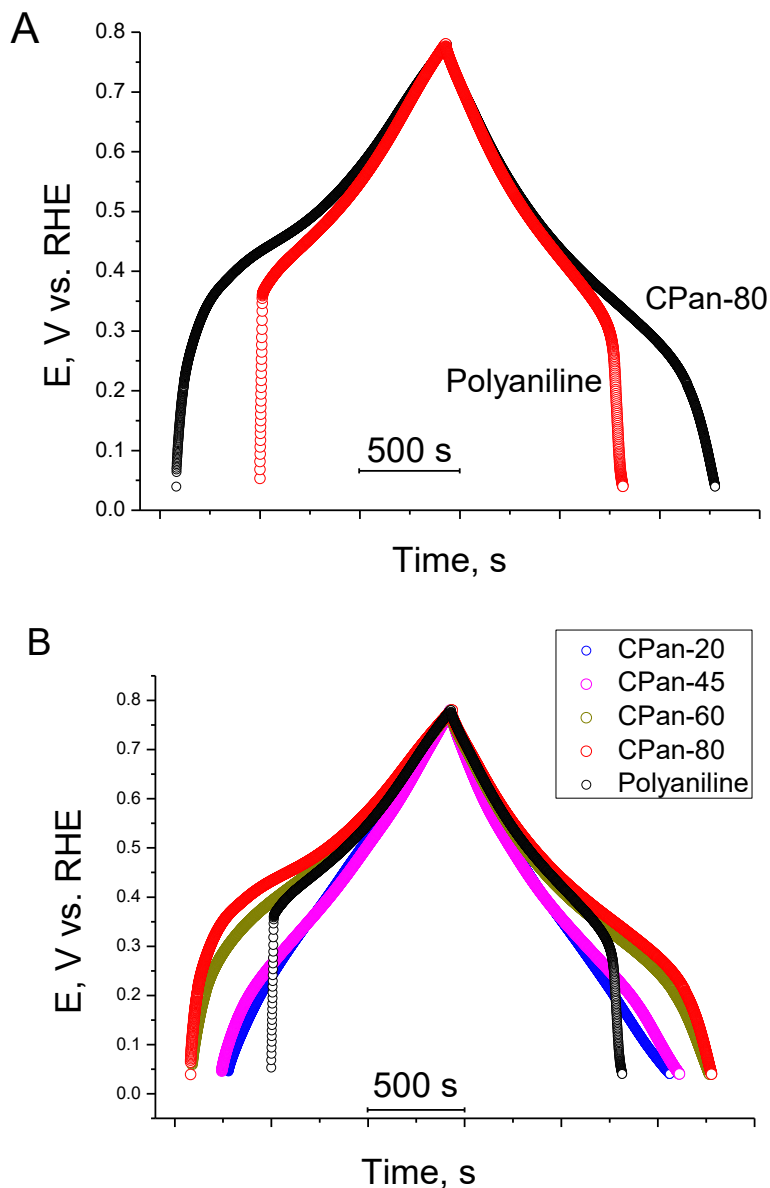


Figure 6. Charge/discharge curves obtained at current density of $0.2 \text{ A} \cdot \text{g}^{-1}$, electrolyte: $1 \text{ M H}_2\text{SO}_4$ (A) Polyaniline and CPan-80 composite; (B) Composite materials

A shape of CVA-curve of the sample with the smallest polymer content – CPan-20 differs from the one of AC CVA-curve insignificantly. The observed poorly identified wide diffuse peak indicates the presence of faradaic processes in the electrode.

Increase in the intensity of peaks at $0.4/0.25$ V potentials is observed for CPan-45 sample, but they are also diffused. Further increase in the polyaniline content yields changes of the anodic peak

shape. It becomes narrower, more pronounced and to be shifted to the anodic region (the same is observed for the cathodic peak) to 0.47/0.38 V potentials. However, further increase in the polymer content does not change the position of the peaks significantly. Only substantial increase of their intensity is observed.

Finally, CV shape of the sample with the highest polymer content CPAn-80 is similar to the shape of the pure polyaniline curve. However, two important differences should be noted: (1) current intensity in potential range 0.05 – 0.45 V is considerable, which can be explained by the presence of the carbon material possessing the substantial electrochemical response in this region; (2) even in the samples with high polyaniline content, the leucoemeraldine/emeraldine transition is shifted to cathodic region as compared to the pure polymer, which is explained by the presence of the carbon material that promotes migration of ions and, accordingly, facilitates the ox-red reactions.

Capacitive properties of composites were determined by chronopotentiometry in potential range of 0.05 – 0.8 V and charge/discharge current densities $0.2 \text{ A} \cdot \text{g}^{-1}$. In the Figure 6, charge/discharge curves of pure polyaniline and the CPAn-80 composite are presented.

On the charge/discharge curves of the pure polyaniline electrode, two regions with different slope angles can be clearly distinguished. The first region (0.05 – 0.3 V) is characterized by a sharp change of the potential almost parallel to the y-axis, indicating a nearly complete absence of electrochemical processes in this region. In the second region (0.3 – 0.8 V), the slope of the curve changes demonstrating the smooth rise of potential, which is typical for charge/discharge processes. Inflection point ($\sim -0.3 \text{ V}$) corresponds to the leucoemeraldine/emeraldine transition (which is also observed in CVA, Figure 5). A character of potential change over time of the composite electrode is generally the same as that of the pure polyaniline one. Moreover, at potentials above -0.3 V , the curves of polyaniline and CM practically coincide indicating that in this potential region, energy accumulation in samples with high polymer content is determined exclusively by faradaic processes. However, the curve slope changes smoother even at lower potentials ($\sim -0.5 \text{ V}$), which leads to the increase in the charge/discharge time and, accordingly, in the capacitance. Thus, in the potential region where the polyaniline electrochemical response intensity is negligible, energy accumulation is caused mainly by charging/discharging of the AC electrical double layer.

Figure 6B shows the charge/discharge curves of the composites obtained with current density $0.2 \text{ A} \cdot \text{g}^{-1}$. For CPAn-20 sample, the curve has the nearly triangular shape close to the shape of AC, indicating dominance of the EDL charge/discharge processes. With the polymer content increasing the shape of the curves gradually changes: they become similar to the curves of pure polyaniline indicating a significant contribution of faradaic processes. With the increase of polyaniline content in CMs, charge/discharge time and, correspondingly, capacitance rise.

Gravimetric capacitance was calculated from the discharge curves by the equation:

$$C = \frac{i \cdot dt}{dE \cdot m},$$

where C (F/g) is the gravimetric capacitance, i (A) – discharge current, t (s) – discharge time, E (V) – potential window, m (g) – electrode mass.

A dependence of specific capacitance at $0.2 \text{ A}\cdot\text{g}^{-1}$ discharge current density on amount of polyaniline in CMs is shown in Fig. 7A. Capacitance of CPAn-20 is $327 \text{ F}\cdot\text{g}^{-1}$ which exceed the ones of AC ($219 \text{ F}\cdot\text{g}^{-1}$) and comparable with the one of pure PANi ($344 \text{ F}\cdot\text{g}^{-1}$), although polymer content is only 18 wt. %. Further increase of the polyaniline amount leads to a gradual increase in gravimetric capacitance, which reaches $465 \text{ F}\cdot\text{g}^{-1}$ for CPAn-80 (60 wt. % of PANi).

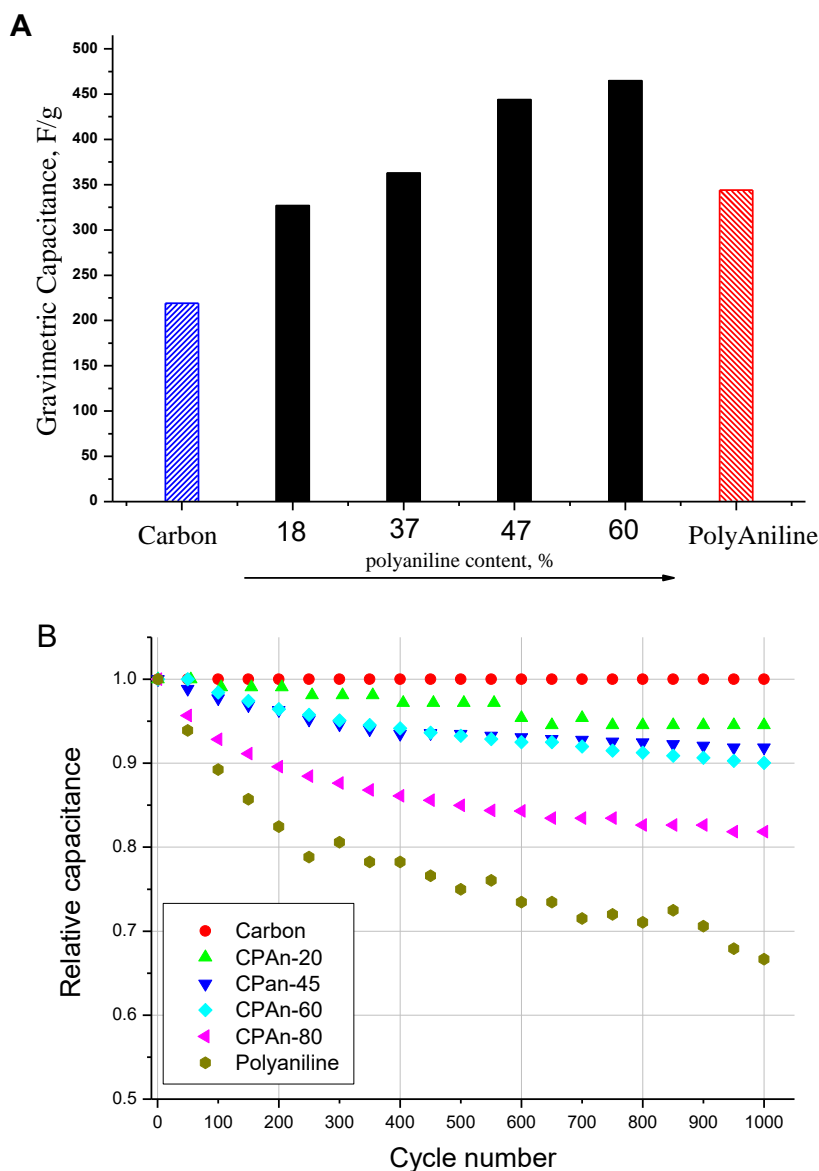


Figure 7. A – Specific capacitance of the carbon/polyaniline composites in dependence on polyaniline content. The data obtained at current density $0.2 \text{ A}\cdot\text{g}^{-1}$; percentages of the PANi content are given based on the NHSC-elemental analysis; B – Dependence of specific capacitance on number of cycles for AC, polyaniline and CMs. The data obtained at current density $3 \text{ A}\cdot\text{g}^{-1}$. Electrolyte – $0.1 \text{ M H}_2\text{SO}_4$.

Capacitive characteristics of the polyaniline composites described in the literature vary in a wide range. Specific capacitance values of the polyaniline/activated carbon composites are in the range of $200\text{--}600 \text{ F}\cdot\text{g}^{-1}$ [19,29–31,36,50]. For example, CM based on the bamboo-carbon possesses

capacitance $277 \text{ F}\cdot\text{g}^{-1}$ at current density $0.5 \text{ A}\cdot\text{g}^{-1}$ [30]. While a composite based on coconut shell carbon has capacitance $534 \text{ F}\cdot\text{g}^{-1}$ at $5 \text{ mV}\cdot\text{s}^{-1}$ sweep rate [31]. Thus, the presented composites based on the rice husk-derived AC show capacitive characteristics comparable or even exceeding the reported in literature.

Changing of specific capacitance with polyaniline amount depends on features of AC, synthesis and way of electrode formation. Some studies reported increase in capacitance rateably with polyaniline content till certain values, beyond which the further PANi adding affected the capacitance negatively. For instance, maximum capacitance $352 \text{ F}\cdot\text{g}^{-1}$ was observed at polyaniline content 18 % for CM based on macroporous carbon, meanwhile CM containing 35 % of PANi had significantly less capacitance – $259 \text{ F}\cdot\text{g}^{-1}$ [12]. Such behavior is explained by formation of a compact thick layer during electrochemical preparation of the electrode, which greatly reduces the efficiency of active species utilization.

A composite based on graphene oxide containing 80 % of PANi prepared by mixing has capacitance less than 50 % PANi composite (668 and $808 \text{ F}\cdot\text{g}^{-1}$, respectively) [27]. The authors explain the observed phenomenon by trespassing of the graphene conductive network with the large amount of the polymer, which leads to the increase of charge-transfer resistance and capacitance decays.

In the present study, specific capacitance increases with polyaniline content. The linear dependence points on formation of a porous structure accessible for the electrolyte ions and providing the transport of ions and electrons.

Specific capacitance of the samples at the different discharge current densities is given in Table 3. Decrease in the gravimetric capacitance occurs with increase of current density for the pure materials and composites. Polyaniline loses almost half of capacitance value (47 %) with increase of the current density from 0.2 to $5 \text{ A}\cdot\text{g}^{-1}$. Degree of the composite capacitance decays is 20-30%, which is comparable with AC (22%).

Table 3. Specific capacitance ($\text{F}\cdot\text{g}^{-1}$) of the activated carbon, polyaniline and composite materials, calculated from discharge curves at the different current densities

Sample	$0.2 \text{ A}\cdot\text{g}^{-1}$	$0.6 \text{ A}\cdot\text{g}^{-1}$	$1 \text{ A}\cdot\text{g}^{-1}$	$3 \text{ A}\cdot\text{g}^{-1}$	$5 \text{ A}\cdot\text{g}^{-1}$
AC	219	200	196	187	172
CPAn-20	327	315	303	300	238
CPAn -45	363	352	344	340	333
CPAn -60	444	434	434	400	357
CPAn -80	465	461	434	365	333
Polyaniline	344	333	294	250	185

The decrease in specific capacitance with increasing in the discharge current density is the phenomenon typical for SC materials. When charging time is shortened, i.e. when the current density increases, a part of the electrode surface becomes inaccessible for electrolyte ions due to diffusion difficulties. Decrease in capacitance is observed for the vast majority of electrode materials and does not depend on an energy storage mechanism. Thereafter, if at slow charging the porosity and surface

availability are not key factors, then as the current density increases, they become crucial. In the case of polyaniline, due to a compactness of its layer, at the high charge/discharge rates, not the entire polymer participates in ox-red conversions, which leads to a significant decrease in capacitance characteristics. However, the presence of AC in a composite greatly facilitates diffusion of the electrolyte ions within the electrode, increasing the degree of the polymer use, which allows accumulation of more energy even at relatively high electrode charging rates.

Stability of an electrode material during long-term use is one of key parameters that determine its prospects for the use in supercapacitors. Figure 7B shows data on stability of AC, polyaniline and composite materials obtained at current density $3 \text{ A}\cdot\text{g}^{-1}$. Specific capacitance of the carbon material for 1000 cycles, as expected, has not been changed. Capacitance change during durability test of CPAn-20 is negligible, only about 6 %. Capacitance decay for CPAn-45 and CPAn-60 containing 37.3 and 47.8 wt.% of the polyaniline respectively, was found to be less than 10 %. Further increase in PANi content results in acceleration of the degradation degree. Specific capacitance of CPAn-80 with 60.7 wt. % PANi was found to reduce by 20 %. The maximal drop, as expected was in the case of PANi electrode – only 65 % capacitance of the initial one was observed.

The observed increase in specific capacitance with the increase in polyaniline amount in the composites cannot be explained by a simple summation of the component capacitances in accordance with their content in the material. Indeed, a simple addition of the PANi and carbon capacitance (219 and $344 \text{ F}\cdot\text{g}^{-1}$) for CPAn-20 and CPAn-80 samples yields values of 247 and $285 \text{ F}\cdot\text{g}^{-1}$, respectively, which is significantly less than the measured values – 327 and $465 \text{ F}\cdot\text{g}^{-1}$. Difference in the calculated and experimental capacitances values are explained by the synergetic effect between polyaniline and carbon. The carbon material used for the synthesis of the composites has highly developed surface and large pore volume (Table 2) and acts as the polymer support. The high surface area of the AC provides uniform distribution of the polymer on the surface, which makes it possible to increase the electrode/electrolyte interface and, accordingly, the surface availability for the electrolyte ions. This increases the degree of the polymer particles use. In addition to optimization of transport processes, the AC serves as a kind of a “pillow” for the mechanical deformation of the polyaniline occurring during ox-red transformations. This allows, if not avoided, significant slowing down the mechanical destruction of the electrode material which confirmed by our observations (Fig. 7B). However, it should be emphasized that polyaniline amount is one of the crucial factor affecting composite stability.

4. CONCLUSIONS

The "carbon/polyaniline" composite materials with different ratio of the components were synthesized by oxidative aniline polymerization in the presence of rice husk-derived activated carbon material. It was shown that the specific capacitance of CMs rises with the increase of the polymer amount, and in all cases, its value exceeds a simple sum of the capacitances of the individual components. Sample possessing a maximal polymer content (60 wt %) was found to have specific capacitance $465 \text{ F}\cdot\text{g}^{-1}$ in $1 \text{ M H}_2\text{SO}_4$ at discharge current density of $0.2 \text{ A}\cdot\text{g}^{-1}$. The used activated carbon having highly developed specific surface area acts as a support on which the polyaniline

particles are distributed. The high surface area of the porous material improves diffusion of the electrolyte ions within the electrode and ensures more complete use of the polymer.

However, durability tests showed that the stability of the composite is determined by the polyaniline content: decrease in capacitance for the sample with 60 % PANi is 20 %, meanwhile capacitances of CMs having less PANi loadings (< 50 wt. %) drops less than by 10 % from their initial ones. This means that the optimal PANi/AC composite material for supercapacitors should be determined based on the balance between high capacitance and long-term stability

Thus, the combination of the activated carbon material and the conductive polymer provides the synergistic effect leading to improved capacitive and operational characteristics and allows consideration of such composite materials as promising for the use as active component of SCs electrodes.

ACKNOWLEDGMENTS

The work is supported by Russian Foundation for Basic Research (project № 17-43-540794).

References

1. A. Burke, *Electrochim. Acta.*, 53 (2007) 1083.
2. M. Conte, *Fuel Cells.*, 10 (2010) 806.
3. Y. Zhang, H. Feng, X. Wu, L. Wang, A. Zhang, T. Xia and H. Dong, X. Li and L. Zhang, *Int. J. Hydrogen Energy.*, 34 (2009) 4889.
4. E. Ito, S. Mozia, M. Okuda, T. Nakano, M. Toyoda and M. Inagaki, *New Carbon Mater.*, 22 (2007) 321.
5. M.P. Bichat, E. Raymundo-Piñero and F. Béguin, *Carbon N. Y.*, 48 (2010) 4351.
6. C. Long, L. Jiang, X. Wu, Y. Jiang, D. Yang, C. Wang, T. Wei and Z. Fan, *Carbon N. Y.*, 93 (2015) 412.
7. C. Peng, X. Bin Yan, R.T. Wang, J.W. Lang, Y.J. Ou and Q.J. Xue, *Electrochim. Acta.*, 87 (2013) 401.
8. M.J. Bleda-Martínez, J.A. Maciá-Agulló, D. Lozano-Castelló, E. Morallón, D. Cazorla-Amorós and A. Linares-Solano, *Carbon N. Y.*, 43 (2005) 2677.
9. E. Raymundo-Piñero, K. Kierzek, J. Machnikowski and F. Béguin, *Carbon N. Y.*, 44 (2006) 2498.
10. X. Lu, H. Dou, B. Gao, C. Yuan, S. Yang, L. Hao, L. Shen and X. Zhang, *Electrochim. Acta.*, 56 (2011) 5115.
11. L.L. Zhang, T. Wei, W. Wang and X.S. Zhao, *Microporous Mesoporous Mater.*, 123 (2009) 260.
12. L.L. Zhang, S. Li, J. Zhang, P. Guo, J. Zheng and X.S. Zhao, *Chem. Mater.*, 22 (2010) 1195.
13. G. Wang, Y. Ling, F. Qian, X. Yang, X.X. Liu and Y. Li, *J. Power Sources.*, 196 (2011) 5209.
14. L. Liu, J. Yang, Y. Jiang, Y. Huang and Q. Meng, *Synth. Met.*, 170 (2013) 57.
15. D. Aradilla, F. Estrany, E. Armelin and C. Alemán, *Thin Solid Films.*, 520 (2012) 4402.
16. J.H. Huang and C.W. Chu, *Electrochim. Acta.*, 56 (2011) 7228.
17. E. Frackowiak, V. Khomenko, K. Jurewicz, K. Lota and F. Béguin, *J. Power Sources.*, 153 (2006) 413.
18. G. Dione, M.M. Dieng, J.J. Aaron, H. Cachet and C. Cachet, *J. Power Sources.*, 170 (2007) 441.
19. X. Ning and W. Zhong, L. Wan, *RSC Adv.*, 6 (2016) 25519.
20. C.C. Hu and J.Y. Lin, *Electrochim. Acta.*, 47 (2002) 4055.
21. J. Tian, D. Peng, X. Wu, W. Li, H. Deng and S. Liu, *Carbohydr. Polym.*, 156 (2017) 19.

22. H. Okamoto and T. Kotaka, *Polymer (Guildf)*, 39 (1998) 4349.
23. E. Salamifar, M.A. Mehrgardi and M.F. Mousavi, *Electrochim. Acta.*, 54 (2009) 4638.
24. S.B. Yoon, E.H. Yoon and K.B. Kim, *J. Power Sources.*, 196 (2011) 10791.
25. H. Zhang, G. Cao, W. Wang, K. Yuan, B. Xu, W. Zhang, J. Cheng and Y. Yang, *Electrochim. Acta.*, 54 (2009) 1153.
26. H. Liu, Y. Wang, X. Gou, T. Qi, J. Yang and Y. Ding, *Mater. Sci. Eng. B Solid-State Mater. Adv. Technol.*, 178 (2013) 293.
27. L. Zhang, D. Huang, N. Hu, C. Yang, M. Li, H. Wei, Z. Yang, Y. Su and Y. Zhang, *J. Power Sources.*, 342 (2017) 1.
28. J. Li, H. Xie, Y. Li, J. Liu and Z. Li, *J. Power Sources.*, 196 (2011) 10775.
29. A. Olad and H. Gharekhani, *J. Polym. Res.*, 23 (2016).
30. X. Zhou, L. Li, S. Dong, X. Chen, P. Han, H. Xu, J. Yao, C. Shang, Z. Liu and G. Cui, *J. Solid State Electrochem.*, 16 (2012) 877.
31. D.S. Patil, S.A. Pawar, R.S. Devan, Y.R. Ma, W.R. Bae, J.H. Kim and P.S. Patil, *Mater. Lett.*, 117 (2014) 248.
32. R.E.O. William S. Hummers, Jr., *J. Am. Chem. Soc.*, 80 (1958) 1339.
33. Y. V. Larichev, P.M. Yeletsky and V.A. Yakovlev, *J. Phys. Chem. Solids.*, 87 (2015) 58.
34. P.M. Eletskaa, V.A. Yakovlev, V.B. Felonov and V.N. Parmon, *Kinet. Catal.*, 49 (2008) 708.
35. P.M. Yeletsky, V.A. Yakovlev, M.S. Mel'gunov and V.N. Parmon, *Microporous Mesoporous Mater.*, 121 (2009) 34.
36. M. V. Lebedeva, P.M. Yeletsky, A.B. Ayupov, A.N. Kuznetsov, V.A. Yakovlev and V.N. Parmon, *Mater. Renew. Sustain. Energy.*, 4 (2015) 1.
37. M. Thommes, K. Kaneko, A. V. Neimark, J.P. Olivier, F. Rodriguez-Reinoso, J. Rouquerol and K.S.W. Sing, *Pure Appl. Chem.*, 87 (2015) 1051.
38. M.S. Mel'gunov and A.B. Ayupov, *Microporous Mesoporous Mater.*, 243 (2017) 147.
39. J. Weber, M. Antonietti and A. Thomas, *Macromolecules.*, 41 (2008) 2880.
40. J. Jeromenok and J. Weber, *Langmuir.*, 29 (2013) 12982.
41. K. Kinoshita, *Carbon: Electrochemical and Physicochemical Properties*, John and Wiley Sons, 1988.
42. C.C. Hu, E. Chen and J.Y. Lin, *Electrochim. Acta.*, 47 (2002) 2741.
43. X.Y. Zhao, J.B. Zang, Y.H. Wang, L.Y. Bian and J.K. Yu, *Electrochem. Commun.*, 11 (2009) 1297.
44. M.S. Rahmanifar, M.F. Mousavi, M. Shamsipur and S. Riahi, *Polym. Degrad. Stab.*, 91 (2006) 3463.
45. V.S. Jamadade and D.S. Dhawale, C.D. Lokhande, *Synth. Met.*, 160 (2010) 955.
46. G. Paasch and P.H. Nguyen, A. J. Fisher, *Chem. Phys.*, 227 (1998) 219.
47. K. Roßberg, G. Paasch, L. Dunsch and S. Ludwig, *J. Electroanal. Chem.*, 443 (1998) 49.
48. I.I. A., S.K. Young, S.S. Jae, I. Hyunsik, K. Hyungsang, K. Dae-Young, S.K. R. and P. Chan Jin, *J. Korean Phys. Soc.*, 59 (2011) 145.
49. K. Aoki and S. Tano, *Electrochim. Acta.*, 50 (2005) 1491.
50. Q. Wang, J.-L. Li, F. Gao, W.-S. Li, K.-Z. Wu and X.-D. Wang, *Carbon N. Y.*, 47 (2009) 353.